Effect of Angle of Attack and Mach Number on Slender-Wing Unsteady Aerodynamics

Lars E. Ericsson* and J. Peter Reding†
Lockheed Missiles and Space Company, Inc., Sunnyvale, Calif.

An analytic theory is presented in which the classical slender wing theory is modified to account for the combined effects of large angle of attack and nonsonic Mach number on the unsteady aerodynamics. The computed results agree well with available static and dynamic experimental data for slender delta wings in the Mach number range $0 \le M_\infty \le 2.8$. The method was extended to compute the unsteady aerodynamics of the space shuttle orbiter by defining an equivalent slender wing using static experimental data. The results obtained in this manner are in good agreement with dynamic experimental results for the Mach number range $0.3 \le M_\infty < 0.95$.

Nomenclature

A	= aspect ratio $= b^2/S$
b	= wingspan
$\bar{c}$	= reference length (mean aerodynamic chord; for a delta wing $\bar{c} = 2c_0/3$)
c_0	= slender-wing root chord
K_{Ma}, K_{MV}	= Mach number parameters, Eqs. (1) and (4)
K_p, K_V	= potential flow and vortex lift factors
L	= lift: coefficient $C_L = L/(\rho_\infty U_\infty^2/2)S$
M	= Mach number
M_p	= pitching moment: coefficient $C_m = M_p/(\rho_\infty U_\infty^2/2)S\bar{c}$
N	= normal force: coefficient $C_N = N/(\rho_\infty U_\infty^2/2)S$
q	= pitch rate
Re	= Reynolds number (based on root chord and freestream conditions)
S	= reference area (= projected wing area)
s	= local semispan
t	= time
T	= period of oscillation
U	= horizontal velocity
$\bar{U}$	= convection velocity
x	= axial body-fixed coordinate
y	= spanwise body-fixed coordinate
α	= angle of attack
α_0	= trim angle of attack
$\bar{\alpha}$	= generalized angle of attack, Eq. (8)
$\bar{\beta}$	= M parameter $= \sqrt{\lvert 1 - M_\infty^2 \rvert}$
Δ	= increment
η	= dimensionless y coordinate $= y/s$
θ	= angular perturbation in pitch
θ_{LE}	= apex half-angle
θ_{TE}	= trailing-edge sweep angle
ξ	= dimensionless x coordinate $= x/c_0$
ρ	= air density
ψ	= phase angle $= \omega t$
$\omega, \bar{\omega}$	= pitching frequency, $\bar{\omega} = \omega\bar{c}/U_\infty$

Subscripts

A	= apex
a	= attached flow
CG	= center of gravity
crit	= critical
D	= discontinuity
EW	= equivalent wing
eff	= effective
LE	= leading edge
SW	= slender wing
s	= separated flow
TE	= trailing edge
V	= vortex
2D	= two-dimensional flow
∞	= freestream conditions

Superscripts

$(\bar{\ })$	= barred quantities denote integrated mean values

Derivative Symbols

$\dot{\theta}$	$= \partial\theta/\partial t$
$C_{N\alpha}$	$= \partial C_N/\partial\alpha$; $C_{m\theta} = \partial C_m/\partial\theta$
$C_{m\dot{\theta}}$	$= C_{mq} + C_{m\dot{\alpha}} = \partial C_m/\partial\,(c\dot{\theta}/U_\infty)$
$C_{\dot{m}\theta}$ and $C_{\dot{m}\dot{\theta}}$	= mean coefficients for nonlinear characteristics, Eqs. (15-17).

Introduction

THE increased operational range of high-performance aircraft and tactical missiles as well as the unique operational requirements of the Space Shuttle Orbiter have created new demands on our understanding of the high-angle-of-attack characteristics of lifting surfaces. This is especially true in regard to the unsteady aerodynamics. In the case of low-aspect-ratio wings with highly swept leading edges, separated flow exhibits itself in the form of leading-edge vortices which affect the aerodynamics throughout the angle-of-attack range and can have a decisive influence on dynamic stability characteristics already at low angles of attack. Using Jones' slender-wing theory[1] and Polyhamus' concept of vortex-induced leading-edge suction loads[2] as starting points, a simple analytic theory was developed that could predict the subsonic unsteady aerodynamics of slender wings at high angles of attack.[3-5] In order to make the developed analytic tools[3-5] applicable to realistic vehicles, such as high-performance aircraft and tactical missiles, or the present

Presented as Paper 77-667 at the AIAA 10th Fluid and Plasmadynamics Conference, Albuquerque, N. Mex., June 27-29, 1977; submitted Oct. 7, 1977; revision received Jan. 31, 1978.

Index categories: Nonsteady Aerodynamics; Aerodynamics.
*Consulting Engineer. Associate Fellow AIAA.
†Research Specialist. Member AIAA.

Space Shuttle Orbiter, the analysis has to be extended into the transonic and supersonic speed regions. This has been done in the present paper. The results obtained are in good agreement with available experimental data.

Analysis

K_P and K_V are constants determining the magnitudes of attached flow and vortex lift components, respectively.[2-5] In Jones' slender-wing theory[1] $(K_P)_{SW}=\pi A/2$. According to Ref. 6, Jones derived a correction for the effect of finite aspect ratio, which in the case of compressible flow can be written

$$K_P=K_{Ma}\cdot(K_P)_{SW} \tag{1a}$$

$$K_{Ma}=2/[1+A\bar{\beta}/4+\sqrt{1+(A\bar{\beta}/4)^2}] \tag{1b}$$

$$\bar{\beta}=\sqrt{|1-M^2|} \tag{1c}$$

This expression for K_{Ma} gives values that agree well with those derived empirically in Ref. 3, the difference being less than 1.5% for $A=1$. Applying Eq.(1) also for supersonic Mach numbers gives slightly lower lift than the inviscid value derived in Ref. 7. At the limit $A\bar{\beta}/4=1$, when the leading edge ceases to be subsonic, the difference is 8%. As it does not seem unreasonable that such a decrease from the two-dimensional inviscid value could be caused by viscous edge conditions, Eq. (1) will be used for both subsonic and supersonic Mach numbers. Thus, in the Mach number range for subsonic leading-edge conditions, $0\le M_\infty\le\sqrt{1+(A/4)^{-2}}$, the formulation for the attached flow aerodynamics is as follows:[3]

$$C_{Na}=(C_{Na})_{SW}K_{Ma} \tag{2a}$$

$$(C_{Na})_{SW}=(\pi A/2)\ \sin\alpha\cos\alpha \tag{2b}$$

$$C_{ma}=-(c_0/\bar{c})C_{Na}(\bar{\xi}_a-\xi_{CG}) \tag{2c}$$

$$K_{Ma}=2[1+A\bar{\beta}/4+\sqrt{1+(A\bar{\beta}/4)^2}]^{-1} \tag{2d}$$

$$\xi_a=\begin{cases}0.667\sqrt{K_{Ma}} & (0\le M_\infty<1)\\ 0.667 & (1\le M_\infty\le\sqrt{1+(A/4)^{-2}}\end{cases} \tag{2e}$$

Polhamus' expression for the vortex lift at supersonic speeds[2] can be written

$$K_V=\pi[1+(A/4)^2]^{1/2}K_{Ma}^2[1-(A\bar{\beta}/4)^2]^{1/2} \tag{3}$$

Thus, the vortex-induced aerodynamics can be approximated as follows:[3-5]

$$C_{NV}=(C_{NV})_{SW}K_{MV} \tag{4a}$$

$$(C_{NV})_{SW}=\pi[1+(A/4)^2]^{1/2}\sin^2(\alpha-\alpha_s) \tag{4b}$$

$$C_{mV}=-(c_0/\bar{c})C_{NV}[0.3(\bar{\xi}_a-\xi_{CG})+0.7(\bar{\xi}_V-\xi_{CG})] \tag{4c}$$

$$K_{MV}=[1-(A\bar{\beta}/4)^2]^{1/2}\begin{cases}1 & (0\le M_\infty<1)\\ K_{Ma}^2 & (1\le M_\infty\le\sqrt{1+(A/4)^{-2}})\end{cases} \tag{4d}$$

$$\bar{\xi}_V=0.587\begin{cases}(1-0.046\bar{\beta})[1-\bar{\eta}_V(A\bar{\beta}/4)^2] & (0\le M_\infty<1)\\ 1 & (1\le M_\infty\le\sqrt{1+(A/4)^{-2}})\end{cases} \tag{4e}$$

$$\bar{\eta}_V=0.56+0.36[1.75+(\alpha/\theta_{LE})]^{-1} \tag{4f}$$

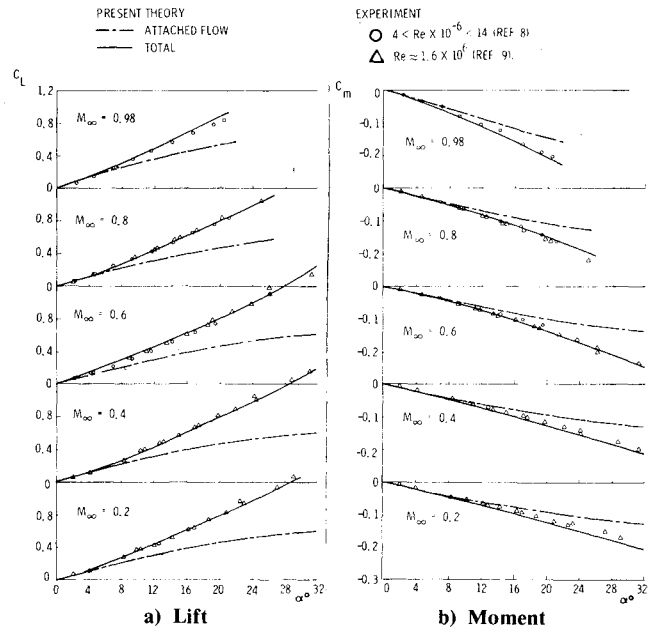

a) Lift b) Moment

Fig. 1 Aerodynamic characteristics of an $A=1.15$ delta wing at subsonic speeds.

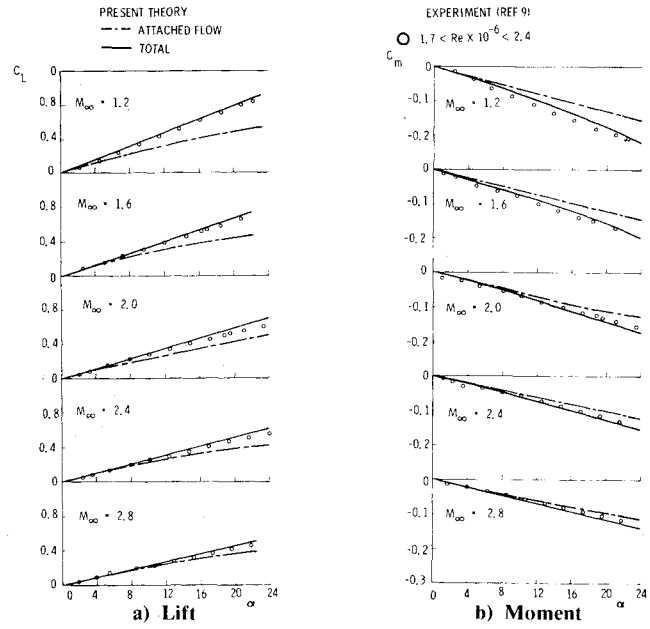

a) Lift b) Moment

Fig. 2 Aerodynamic characteristics of an $A=1.15$ delta wing at supersonic speeds.

The predictions obtained by use of Eqs. (2) and (4) are compared with experimental data[8,9] in Figs. 1 and 2. It can be seen that the predictions are in good agreement with the experimental results. Especially gratifying is the good agreement with experiment for supersonic speeds (Fig. 2). In Ref. 5 a simple method was derived to account for moderately swept (forward or back) trailing edges. Two equivalent delta wings were defined, one for attached flow loads and another for the vortex-induced loading. These equivalent delta-wing characteristics were referenced ("back") to true wing geometry by multiplication through the following ratios:‡

$$\frac{C_N}{(C_N)_{EW}}=\frac{1-\tan\theta_{LE}\tan\theta_{TE}}{(1-\bar{\eta}\tan\theta_{LE}\tan\theta_{TE})^2} \tag{5a}$$

‡For the present, the incompressible spanwise load center is used for all Mach numbers.

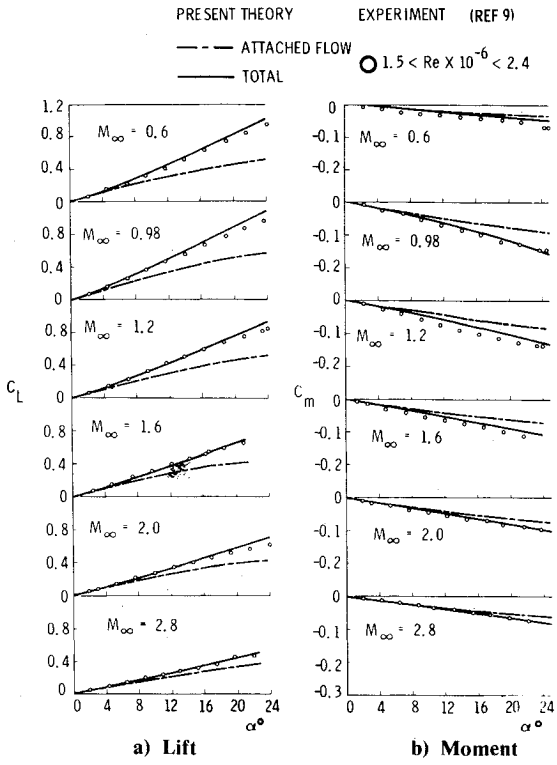

Fig. 3 Aerodynamic characteristics of an $A = 1.47$ arrow wing.

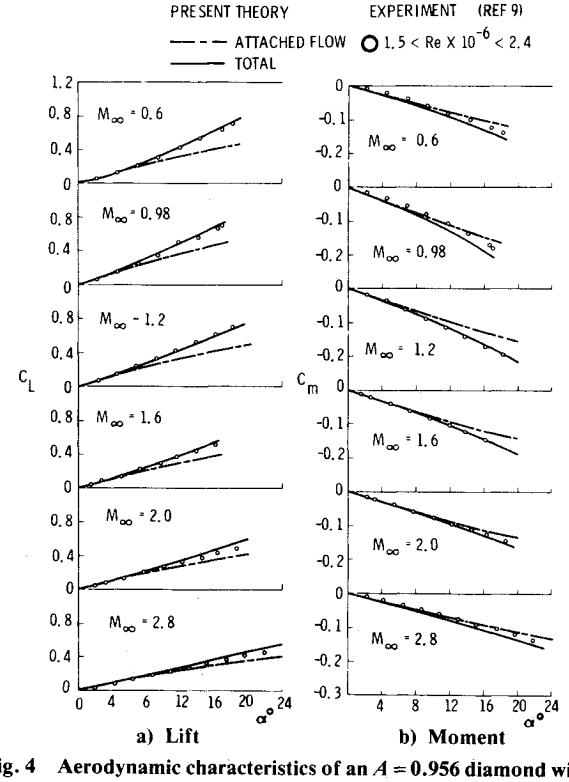

Fig. 4 Aerodynamic characteristics of an $A = 0.956$ diamond wing.

$$c_0/(c_0)_{EW} = (1 - \bar{\eta}\tan\theta_{LE}\tan\theta_{TE}) \tag{5b}$$

$$\bar{\eta}_a = 4/3\pi \tag{5c}$$

Combining Eqs. (2, 4, and 5) gives the results shown in Figs. 3 and 4, indicating that the simple Eq. (5) suffices even when the trailing-edge sweep angles are of significant magnitudes.

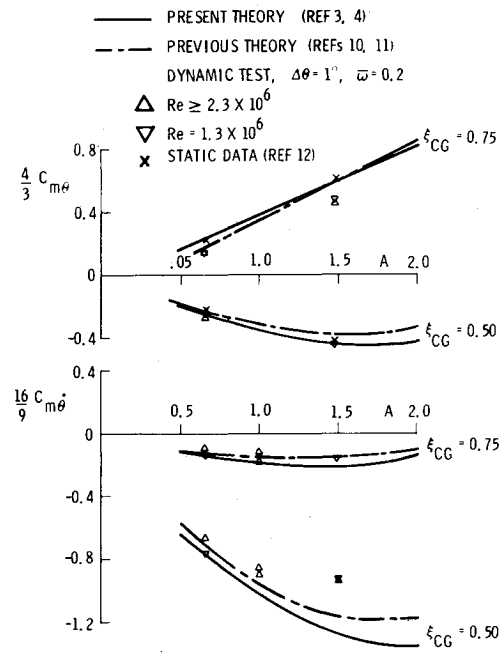

Fig. 5 Effect of aspect ratio on delta-wing pitch damping at $M_\infty = 0$ and $\alpha = 0$.

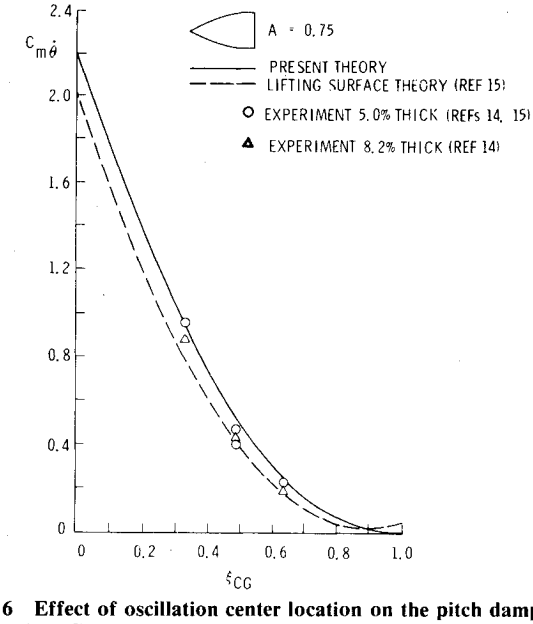

Fig. 6 Effect of oscillation center location on the pitch damping of an $A = 0.75$ Gothic wing at $M_\infty = 0$ and $\alpha = 0$.

Unsteady Aerodynamics

The unsteady aerodynamic characteristics for a delta wing in incompressible flow were derived in Ref. 3. In the present notation the attached flow derivatives are

$$C_{m\theta a} = (c_0/\bar{c})\,C_{N\theta a}\cos^2\alpha_0\,[\bar{\xi}_a - \xi_{CG}] \tag{6a}$$

$$C_{m\dot{\theta}a} = (c_0/\bar{c})^2\,C_{N\theta a}\cos\alpha_0\,[(c_{\text{eff}}/c_0) - \xi_{CG}]^2 \tag{6b}$$

$$C_{N\theta a} = (\pi A/2)\,K_{Ma} \tag{6c}$$

$$c_{\text{eff}}/c_0 = [K_{Ma}(2 - \cos^{-2}\alpha_0)]^{1/2} \tag{6d}$$

and the vortex-induced contributions are

$$C_{m\theta s} = -(c_0/\bar{c})\,C_{N\theta V}[0.3(\bar{\xi}_a - \xi_{CG}) + 0.7(\bar{\xi}_V - \xi_{CG})] \tag{7a}$$

$$C_{m\dot{\theta}s} = -(c_0/c)^2 C_{N\theta V}\{0.3\sec\alpha_0[(c_{\text{eff}}/c_0) - \xi_{CG}]^2 + 0.7(U_\infty/\bar{U})\bar{\xi}_{CG}(\bar{\xi}_V - \xi_{CG})\} \quad (7b)$$

$$C_{N\theta V} = \pi K_{MV} \sin 2(\alpha_0 - \alpha_s)[1 + (A/4)^2]^{1/2} \quad (7c)$$

The incompressible stability derivatives at $\alpha_0 = 0$ determined by use of Eqs. (2) and (6) are compared with experimental results in Figs. 5 and 6. Although the account given by the simplified present formulation of the effect of aspect ratio is not as good as the original method of Ref. 1, when compared with experiments,[10-12] the difference is less than 10% (Fig. 5).§ Noticing that both $C_{m\theta}$ and $C_{m\dot{\theta}}$, as measured in the dynamic test of the $A = 1.458$ wing, are 25% below the prediction, whereas the static test gave a stability derivative $C_{m\theta}$ that agrees with the prediction, it is hard to judge how good the present prediction of the aspect ratio effect is. That the prediction is good for low aspect ratios is confirmed by the results shown in Fig. 6 for an $A = 0.75$ Gothic wing. The present prediction of the effect of oscillation center on $C_{m\dot{\theta}}$ agrees with experimental results[13,14] as well as with the computations from lifting surface theory.[15] Figure 7 shows that the prediction of Mach number effects for an $A = 1.45$ delta wing agrees well with experimental data[16] for the subsonic speed range, and also agrees well with other theories[17-19] in the supersonic speed range. The poor agreement between experiment and theory at supersonic speeds could be due to shock-wave/boundary-layer interaction at the trailing edge of the half model, as is suggested in Ref. 16. A similar and probably stronger shock/boundary-layer interaction might explain the sharp dropoff of the damping when the sonic speed is exceeded. According to the results in Ref. 20, the aspect ratio is too low for the wing to realize any of the degraded damping at low supersonic speeds caused by inviscid $\dot{\alpha}$ effects. In Fig. 8 comparison is made with wind-tunnel test data on a sting-mounted $A = 2$ delta wing. Although the aspect ratio is rather high, the present predictions agree well with experimental data[20,21] and available theory.[20] It can be seen that the transonic behavior of the experimental data is not as violent as for the half-model data in Fig. 7. However, even wing-mounted models can experience data distortion due to support interference,[22] especially if boundary-layer transition is occurring on or near the sting/model juncture.[23] The subsonic test data[21] in Fig. 8 were obtained using a very large-diameter sting and support interference is a distinct possibility. At supersonic speeds support interference is less of a problem. All in all, the experimental data in Fig. 8 probably provide a good representation of the correct Mach number trend. In Fig. 9a free-flight data[24] for an $A = 0.865$ Gothic wing are shown to compare well with present predictions. There is also good agreement between present theory and other available supersonic[25,26] and subsonic[27] theories.

The main purpose of the present analysis is to provide simple analytic means for computation of the contribution to the dynamic stability derivatives from the leading-edge vortices that are generated at nonzero angles of attack. Combining Eqs. (2, 4, 6, and 7), the results shown in Fig. 10 were obtained. It can be seen that the vortex-induced effects measured on an $A = 1.458$ delta wing with sharp[10] and rounded[28] leading edges are well predicted. Note that the vortex-induced contributions affect static and dynamic stability in opposite ways, decreasing static stability while increasing the damping. There does not appear to exist any transonic or supersonic dynamic experimental data for delta wings (with subsonic leading edges) at high angles of attack.[29]

§The ordinate scale reflects the fact that $\bar{c} = c_0/2$ was used in Refs. 10-12. In order to avoid confusion the definition in the Nomenclature will be followed strictly, and when the data taken from another data source defines the derivatives in a different manner, this fact will be reflected as shown in Fig. 5.

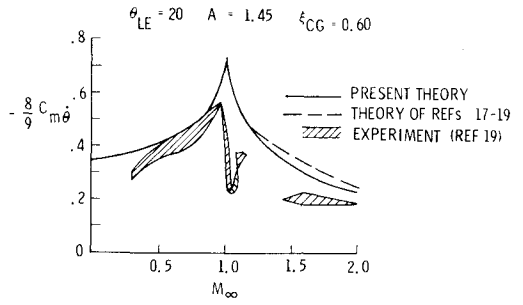

Fig. 7 Effect of Mach number on the pitch damping of an $A = 1.45$ delta wing at $\alpha = 0$.

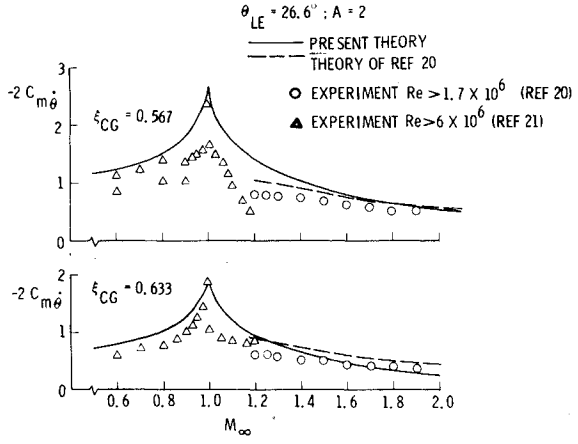

Fig. 8 Effect of Mach number on the pitch damping of an $A = 2$ delta wing at $\alpha = 0$.

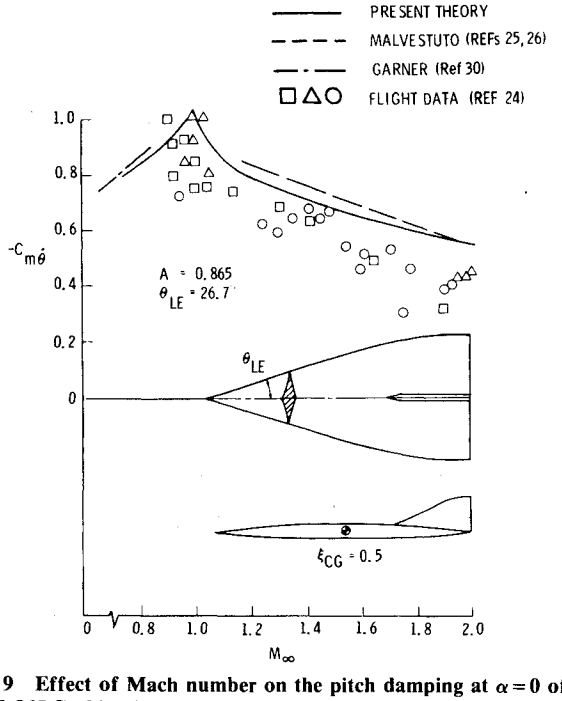

Fig. 9 Effect of Mach number on the pitch damping at $\alpha = 0$ of an $A = 0.865$ Gothic wing.

Thus, a direct comparison, such as in Fig. 10, cannot be made for higher Mach numbers. However, based upon the good agreement with static data, shown in Figs. 1 through 4, one would expect that the present analytic method can provide a good estimate of the unsteady aerodynamics through the complete speed region up to leading-edge shock attachment, $0 \le M_\infty \le \sqrt{1 + (A/4)^{-2}}$.

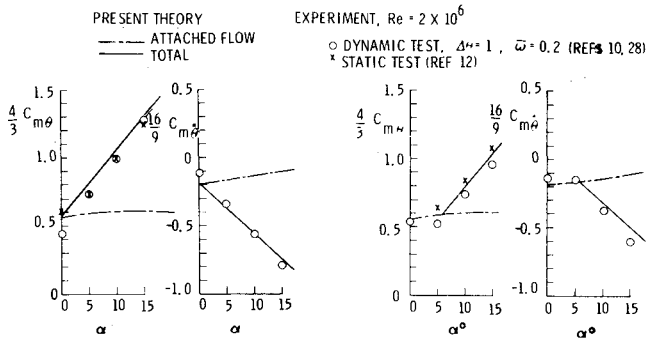

a) Sharp leading edge b) Rounded leading edge

Fig. 10 Effect of angle of attack and leading-edge roundness on the unsteady aerodynamics of an $A = 1.484$ delta wing at $M_\infty = 0$.

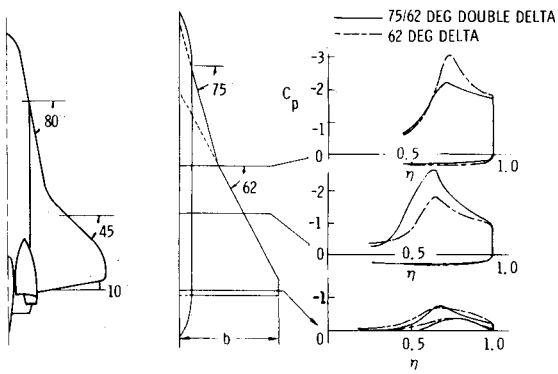

a) Orbiter planform b) Strake-induced loads[30]

Fig. 11 Double-delta planforms.

Orbiter Dynamics

When trying to extend the analytic methods developed for the delta wing to apply to the Space Shuttle Orbiter, one encounters several complications. First, the orbiter has a double-delta wing planform (Fig. 11a). The inner delta wing or strake induces a substantial loading on the main wing[30] (Fig. 11b). In addition to the complication introduced by the strake, there is a considerable influence by the orbiter fuselage. The absence of any wing-body fairing causes flow separation to occur in the wing-fuselage juncture, starting just forward of the OMS pods at $\alpha = 0$. This "axial corner flow" separation grows with increasing angle of attack as crossflow-induced collection of forebody boundary layer "spills" over the strake into the wing-body juncture.[31,32] The addition of low-energy boundary layer to the corner flow region causes the flow separation to grow, occurring closer to, and finally at the strake apex. The separation is vented by a vortex which generates lift on the aft main wing. This vortex is similar to the free body vortices generated on slender bodies of revolution.[33] Thus, the crossflow over the forebody and strake determines the vortex-induced lift on the aft main wing. At high angles of attack the corner vortex interacts with the main wing vortex to form one large-size vortex, which is swept outboard to the outer wing panel where, when some critical angle of attack is exceeded, it starts to burst over the wing, initiating the loss of lift associated with three-dimensional slender-wing stall.

The unsteady aerodynamic characteristics of the orbiter are computed in the following manner. An equivalent slender wing is defined for computation of the attached-flow unsteady aerodynamics, similar to what was done in the delta-wing analysis. The trailing edge of the equivalent wing is located such that the computed slender-wing force derivative $C_{N\alpha a}$ at $\alpha = 0$ agrees with $C_{N\alpha}$ measured in static tests. That determines c_{eff}/c_0 in Eq. (6) and is used to obtain the attached-flow damping derivative $C_{m\dot{\theta}a}$. The corresponding static stability derivative $C_{m\theta a}$ is computed from Eqs. (2) and (6) as $C_{m\theta a}(\alpha) = C_{m\theta a}(0)\cos^2\alpha$, where $C_{m\theta a}(0)$ is $C_{m\alpha}$ at $\alpha = 0$ measured in the static test. The vortex-induced loads are defined as the difference at angle of attack between the actually measured static characteristics[34] and the computed attached-flow characteristics.

In this manner the flow complications caused by the fuselage are accounted for in regard to the magnitude of the vortex-induced loads. In order to obtain the unsteady aerodynamics one has to determine the phasing of these vortex-induced loads. The situation is different from that for the pure delta-wing analysis. For the strake vortex and its induced loads on the strake of a pure double-delta wing (Fig. 11b), the delta-wing analysis would apply. However, for the vortex-induced loads on the main orbiter wing (Fig. 11a), the delta-wing analysis does not apply. The vortex is a free vortex, like a forebody vortex[31-33] or a part-span vortex.[35] Its strength is determined by the feeding from the strake, and the change of vortex strength is convected downstream with freestram speed, $U = U_\infty$. Furthermore, the fuselage cannot be treated as a reflection plane. The corner flow vortex is fed by forebody crossflow. It appears reasonable that the combined crossflow effects can be represented in lumped form by the crossflow at strake apex.[31,32] That is, the vortex-induced force C_{NV} at a station $x - x_A$ downstream of strake apex is a function of the angle of attack at strake apex a time increment Δt earlier, where $\Delta t = (x - x_A)/U_\infty$. For rigid-body oscillations around x_{CG} the generalized angle of attack at strake apex (x_A) is

$$\tilde{\alpha}_A = \alpha_0 + \theta + (x_A - x_{CG})\dot{\theta}/U_\infty \tag{8}$$

With θ being the infinitesimal amplitude perturbation in pitch around α_0 at a low reduced frequency, one can represent $\tilde{\alpha}_A$ $(t - \Delta t)$ by the first-order terms in a Taylor expansion:

$$\tilde{\alpha}_A(t - \Delta t) = \alpha_0 + \theta - \dot{\theta}\Delta t + (x_A - x_{CG})\dot{\theta}/U_\infty \tag{9}$$

The vortex-induced load at x at time t is

$$\Delta C_{NV}(t) = \Delta C_{NV}(\alpha_0) + \Delta C_{N\alpha V}(\alpha_0)\tilde{\alpha}_A(t - [x - x_A]/U_\infty) \tag{10}$$

Combining Eqs. (9) and (10) gives

$$\Delta C_{NV}(t) = \Delta C_{NV}(\alpha_0) + \Delta C_{N\alpha V}(\alpha_0) \times [\theta + (2x_A - x - x_{CG})\dot{\theta}/U_\infty] \tag{11}$$

For the vortex-induced total load centered at $\bar{x}_V$, Eq. (11) gives

$$C_{NV}(t) = C_{NV}(\alpha_0) + C_{N\theta V}\theta + C_{N\dot{\theta}V}(\bar{c}\dot{\theta}/U_\infty) \tag{12a}$$

$$C_{N\theta V} = C_{N\alpha V}(\alpha_0) \tag{12b}$$

$$C_{N\dot{\theta}V} = C_{N\theta V}(2x_A - \bar{x}_V - x_{CG})/\bar{c} \tag{12c}$$

Thus, with $C_{mV} = -C_{NV}(\bar{x}_V - x_{CG})/\bar{c}$, the moment derivatives become

$$C_{m\theta V} = -C_{N\theta V}(\bar{x}_V - x_{CG})/\bar{c} \tag{13a}$$

$$C_{m\dot{\theta}V} = -C_{m\theta V}(\bar{x}_V + x_{CG} - 2x_A)/\bar{c} \tag{13b}$$

As in the case of the pure delta wing (Fig. 10), the vortex-induced loads affect static and dynamic stability in opposite ways. This vortex contribution is added to the attached-flow derivatives for angles of attack $\alpha > \alpha_V$ where the strake-

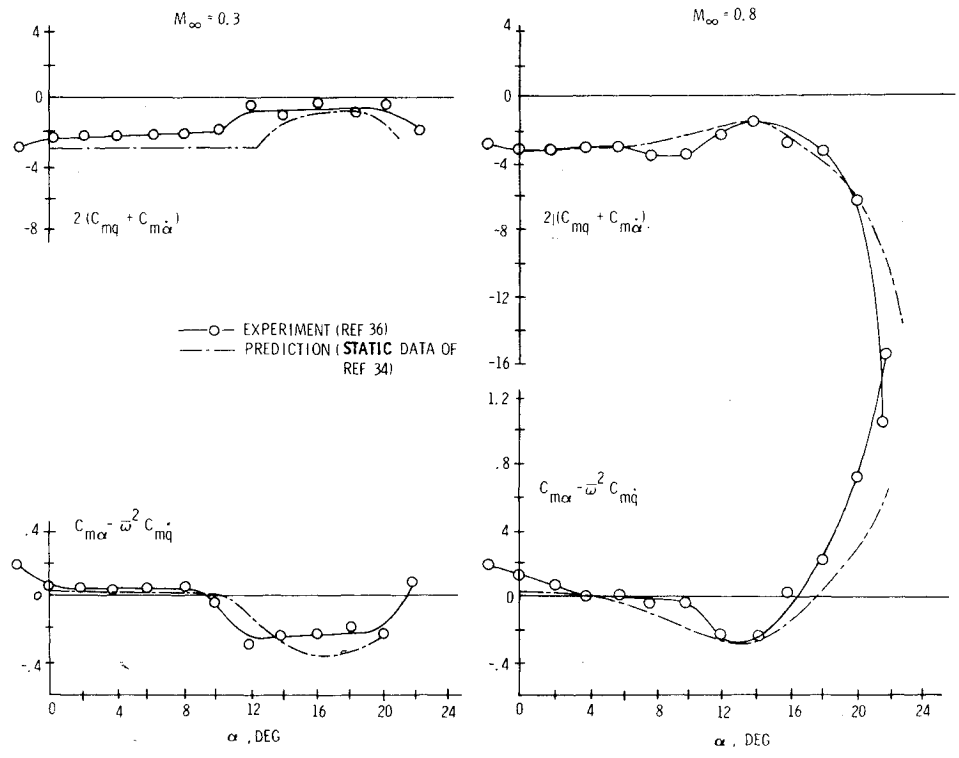

Fig. 12 Orbiter dynamics at subsonic speeds.

fuselage vortex occurs. Thus, the total derivatives are

$$C_{m\theta} = \begin{cases} C_{m\theta a} & (\alpha < \alpha_V) \\ C_{m\theta a} + C_{m\theta V} & (\alpha \geq \alpha_V) \end{cases} \tag{14a}$$

$$C_{m\dot{\theta}} = \begin{cases} C_{m\dot{\theta}a} & (\alpha < \alpha_V) \\ C_{m\dot{\theta}a} + C_{m\dot{\theta}V} & (\alpha \geq \alpha_V) \end{cases} \tag{14b}$$

$$C_{m\theta a} = -C_{N\alpha a}\cos^2\alpha_0 (\bar{x}_a - x_{CG})/\bar{c} \tag{14c}$$

$$C_{m\dot{\theta}a} = -C_{N\alpha a}\cos\alpha_0 [(x_{TE})_{\text{eff}} - x_{CG}]^2/\bar{c}^2 \tag{14d}$$

$$C_{m\theta V} = -C_{N\alpha V}(\bar{x}_V - x_{CG})/\bar{c} \tag{14e}$$

$$C_{m\dot{\theta}V} = -C_{m\theta V}(\bar{x}_V + x_{CG} - 2x_A)/\bar{c} \tag{14f}$$

In Fig. 12 the predicted stability derivatives obtained through Eq. (14) are compared with subsonic dynamic experimental results.[36] The agreement is gratifying. At high angles of attack, $\alpha > 12$ deg, the combined strake-body vortex starts to burst at the trailing edge. As the burst location moves forward with increasing angles of attack, the lift loss increases resulting in a loss of static stability.

Because of the time lag, the effect on the dynamic stability is the opposite, Eq. (13), and the damping is increased. The static data[3,4] used for the dynamic prediction were obtained with a different OMS-pod configuration.¶ Inspection of Fig. 12, keeping the preceding time lag effect in mind, reveals that if the correct static data had been available (they would have coincided with the dynamic $C_{m\alpha}$ data, note that $\bar{\omega}^2 \ll 1$) improved agreement would result between predicted and measured damping characteristics at high angles of attack.

At transonic speed a shock emanates from the corner separation and extends outboard over the wing.[31,32] At some critical angle of attack the wing-body corner separation jumps discontinuously to the strake apex in response to the increase

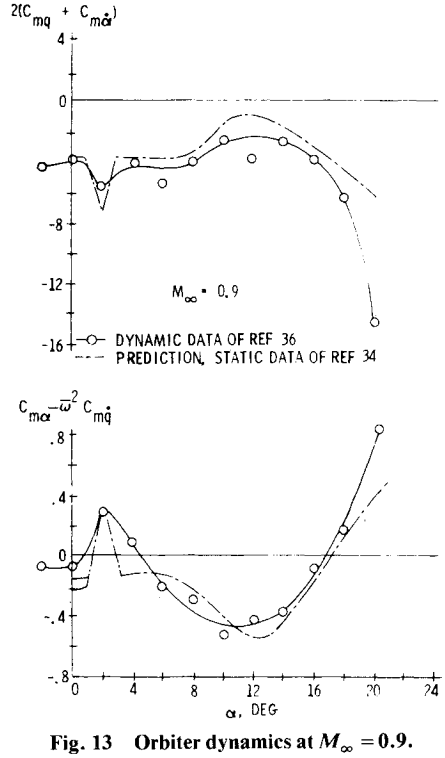

Fig. 13 Orbiter dynamics at $M_\infty = 0.9$.

of the crossflow at strake apex above the critical value. This, in turn, causes the shock to jump forward close to the leading edge of the main wing resulting in a sudden discontinuous change in the wing loading. Thus, the crossflow at the strake apex determines the separation-induced discontinuous load change and its effects on the vehicle dynamics. However, because of the discontinuous variation of the aerodynamic forces the derivative concept, Eq. (14), has to be abandoned. An equivalent effective derivative that varies with the amplitude can be defined which agrees with the derivative-representation in dynamic experiments.[37,38] With ΔC_m being the discontinuous moment jump which occurs when α exceeds

¶The pod containing the Orbital Maneuver System is very bulbous (it can be seen in Fig. 11a, located at the root of the orbiter fin) and has a significant effect on the orbiter aerodynamics.

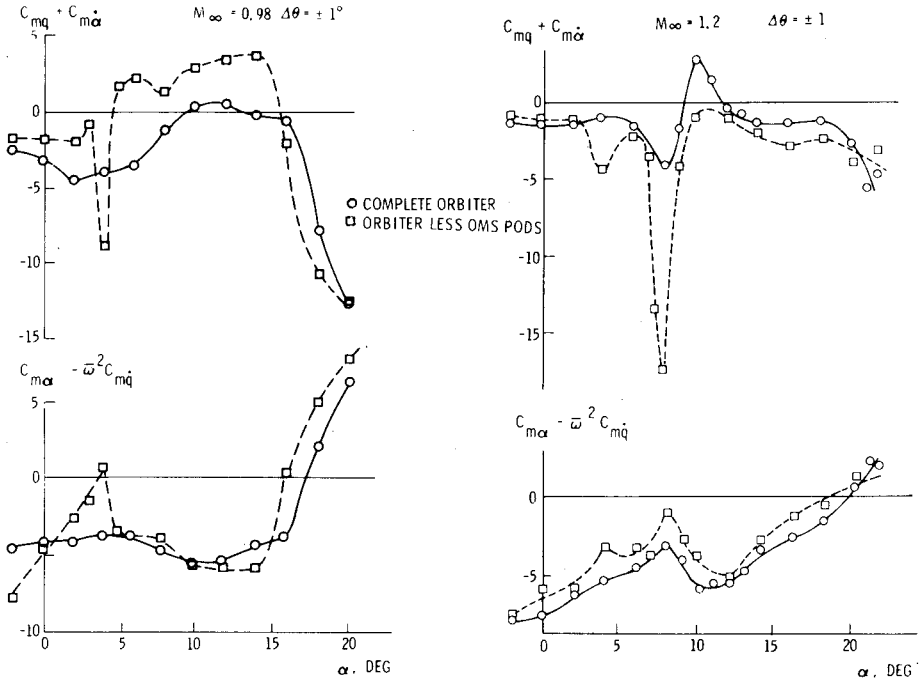

Fig. 14 Effect of OMS-pods on orbiter dynamics at $M_\infty = 0.98$ and $M_\infty = 1.2$.

α_D, one obtains the following effective aerodynamic spring coefficient for pitch oscillations around α_0 of amplitude $\Delta\theta$:

$$C_{\dot{m}\theta} = \frac{1}{\Delta\theta^2}\int_{-\Delta\theta}^{\Delta\theta} C_m \mathrm{d}\theta = C_{m\alpha a} + \frac{\Delta C_m}{\Delta\theta}\left[1 - \frac{\alpha_D - \alpha_0}{\Delta\theta}\right] \quad (15)$$

provided that $\alpha_0 \le \alpha_D \le \alpha_0 + \Delta\theta$. Likewise, the equivalent damping derivative is obtained by integrating the work over one cycle:

$$C_{\dot{m}\dot{\theta}} = \frac{1}{\pi\Delta\theta\bar{\omega}}\int_{\psi_0}^{\psi_0 + 2\pi} C_m(\psi)\cos\psi \mathrm{d}\psi \quad (16)$$

where $\psi = \omega t$ and $\omega T = 2\pi$, with ω and T being the frequency and period of the pitch oscillation. Integration gives

$$C_{\dot{m}\dot{\theta}} = C_{\dot{m}\dot{\theta}a} - \frac{2\Delta C_m}{\pi\Delta\theta}\frac{\bar{x}_V + x_{CG} - 2x_A}{\bar{c}} \quad (17)$$

As the static data[34] did not have the resolution needed to determine ΔC_m, it was determined from the dynamic measurements of $C_{m\alpha}$ using Eq. (15). The ΔC_m value obtained in this manner[33] was used in Eq. (17) to determine the corresponding damping spike. For the rest of the angle-of-attack range, $\alpha_0 < \alpha_D - \Delta\theta$ and $\alpha_0 > \alpha_D + \Delta\theta$, Eq. (14) applies. In Fig. 13 the computed results for $M_\infty = 0.9$ are compared with the Langley damping measurements.[37] The agreement is as good as for the lower Mach numbers in Fig. 12, and would have been even better if the correct static data had been available. This conclusion is based upon the same observation that was applied earlier to the results in Fig. 12.

In the sonic and low supersonic portion of the transonic speed range the flow separation becomes very sensitive to the OMS-pod configuration[31,32,39,40] (Fig. 14), and the error incurred by using the incorrect static data becomes more severe than at the lower Mach numbers. However, even with access to the correct static data it may not be possible to predict the dynamic characteristics using the present approach. The results in Fig. 14 indicate that the separation-induced unsteady loads at $M_\infty = 1.2$ have a more complicated character than what is represented by the present formulation, which is based upon the assumption that the crossflow at strake apex controls the separation-induced loads. Further work is needed to pinpoint the reason for the loss of dynamic stability at transonic speeds, for 8 deg $< \alpha <$ 14 deg at $M_\infty = 0.98$ and for 8 deg $< \alpha <$ 12 deg at $M_\infty = 1.2$ (Fig. 14). When one considers how difficult it is to extrapolate from transonic subscale dynamic test data to full scale[41,42] the dynamic characteristics shown in Fig. 14 give cause for concern.

Conclusions

The presented analysis shows how the classical slender-wing theory can be extended to provide the analytic means needed for computation of the unsteady aerodynamics of present high-performance vehicles operating at high angles of attack. The results are as follows.

1) The effect of Mach number for a subsonic leading edge is accounted for by a simple modification of Jones' slender-wing theory for the attached-flow loads and by an extension of Polhamus' theory for the vortex-induced loads.

2) The effect of moderate trailing-edge sweep (forward or back) is accounted for by the use of two equivalent delta wings, one for the attached-flow loads and another for the vortex-induced loads.

3) Static and dynamic longitudinal aerodynamic characteristics determined by the presented closed-form solutions are in good agreement with available experimental data in the complete Mach number range $0 \le M_\infty \le 2.8$.

4) In the α-M_∞ regions where other theoretical methods exist, they give results that are in close agreement with present predictions.

5) The slender-wing analysis is extended as follows to the Space Shuttle Orbiter wing with its double-delta planform. The attached flow loads are given by an equivalent slender wing that gives the $C_{N\alpha}$ and $C_{m\alpha}$ at $\alpha = 0$ which was measured in static tests. The vortex-induced loads are defined as the difference at $\alpha > 0$ between the measured total static loads and the computed attached-flow loads. The crossflow effects on the unsteady vortex-induced loads are represented in lumped form by the crossflow at the strake apex.

6) The unsteady aerodynamic characteristics of the orbiter computed in this manner are in good agreement with dynamic experimental results in the Mach number range $0.3 \le M_\infty \le 0.9$. At transonic speeds, however, the experimentally observed dynamic instability could not be predicted. Thus, further work is needed in the critical Mach number range $0.95 < M_\infty < 1.4$.

Acknowledgment

The results presented herein were obtained in a study for NASA, Contract NAS 8-30652, under the direction of W. W. Clever, NASA MSFC and J. C. Young, NASA JSC.

References

[1] Jones, R. T., "Properties of Low-Aspect-Ratio Pointed Wings at Speeds Below and Above the Speed of Sound," NACA Rept. 835, 1945.

[2] Polhamus, E. C., "Prediction of Vortex-Lift Characteristics by a Leading-Edge Suction Analogy," *Journal of Aircraft*, Vol. 8, April 1971, pp. 193-199.

[3] Ericsson, L. E. and Reding, J. P., "Unsteady Aerodynamics of Slender Delta Wings at Large Angles of Attack," *Journal of Aircraft*, Vol. 12, Sept. 1975, pp. 721-729.

[4] Ericsson, L. E. and Reding, J. P., "Errata: Unsteady Aerodynamics of Slender Delta Wings at Large Angles of Attack," *Journal of Aircraft*, Vol. 14, Aug. 1977, p. 832.

[5] Ericsson, L. E. and Reding, J. P., "Approximate Nonlinear Slender Wing Aerodynamics," *Journal of Aircraft*, Vol. 14, Dec. 1977, pp. 1197-1204.

[6] Lomax, H. and Sluder, L., "Chordwise and Compressibility Corrections to Slender-Wing Theory," NACA Rept. 1105, 1952.

[7] Brown, C. E., "Theoretical Lift and Drag of Thin Triangular Wings at Supersonic Speeds," NACA Rept. 839, 1946.

[8] Davenport, E. E. and Huffman, J. K., "Experimental and Analytical Investigation of Subsonic Longitudinal and Lateral Aerodynamic Characteristics of Slender Sharp-Edge 74° Swept Wings," NASA TN D-6344, 1971.

[9] Davenport, E. E., "Aerodynamic Characteristics of Three Slender Sharp-Edge 74° Swept Wings at Subsonic, Transonic, and Supersonic Mach Numbers," NASA TN D-7631, 1974.

[10] Woodgate, L. and Pugh, P. G., "Measurements of the Oscillatory Pitching Moment Derivatives on a Slender Sharp-Edged Delta Wing in Incompressible Flow," Aeronautics Research Council, Great Britain, R&M No. 3628, Pt. 2, 1968.

[11] Woodgate, L. and Pugh, P. G., "Measurements of Pitching-Moment Derivatives on a Sharp-Edged Delta Wing in Incompressible Flow," Aeronautics Research Council, Great Britain, R&M No. 3379, 1963.

[12] Woodgate, L. and Halliday, A. S., "Measurements of Lift, Drag, and Pitching Moments on a Series of Three Delta Wings," Pt. 4, Aeronautics Research Council, Great Britain, R&M No. 3628, 1968.

[13] Wright, J. G. and Wilkinson, A., "Low Speed Wind-Tunnel Measurements of Oscillatory Derivatives for a Family of Slender Wings, Part II, Damping in Pitch," Bristol Aircraft Ltd., Rept. W. T. 348, 1960.

[14] Wright, J. G., "Low Speed Wind-Tunnel Measurements of the Oscillatory Longitudinal Derivatives of a Gothic Wing of Aspect Ratio 0.75," Aeronautics Research Council, Great Britain, A.R.C. 24, 357, 1962.

[15] Garner, H. C. and Lehrian, D. E., "Pitching Derivatives for a Gothic Wing Oscillating About a Mean Incidence," Aeronautics Research Council, Great Britain, C.P. No. 695, 1963.

[16] Orlik-Rückemann, K. and Olsson, C. O., "A Method for the Determination of the Damping-in-Pitch of Semi-Span Models in High-Speed Wind-Tunnels, and Some Results for a Triangular Wing," The Aeronautics Research Institute of Sweden, Rept. 62, 1956.

[17] Ribner, H. S. and Malvestuto, F. S. Jr., "Stability Derivatives of Triangular Wings at Supersonic Speeds," NACA Rept. 908, 1948.

[18] Watkins, C. E. and Berman, J. H., "Airforces and Moments on Triangular and Related Wings with Subsonic Leading Edges Oscillating in Supersonic Potential Flow," NACA Rept. 1099, 1952.

[19] Berndt, S. B., "On the Theory of Slowly Oscillating Delta Wings at Supersonic Speeds," The Aeronautics Research Institute of Sweden, Rept. 43, 1951.

[20] Tobak, M., "Damping in Pitch of Low-Aspect-Ratio Wings at Subsonic and Supersonic Speeds," NACA RM A52LO4a, 1953.

[21] Emerson, H. F. and Robinson, R. C., "Experimental Wind Tunnel Investigation of the Transonic Damping-in-Pitch Characteristics of Two Wing-Body Combinations," NASA Memo 11-30-58A, 1958.

[22] Reding, J. P. and Ericsson, L. E., "Dynamic Support Interference," *Journal of Spacecraft and Rockets*, Vol. 9, July 1972, pp. 547-553.

[23] Ericsson, L. E. and Reding, J. P., "Boundary-Layer Transition and Dynamic Sting Interference," *AIAA Journal*, Vol. 8, Oct. 1970, pp. 1886-1888.

[24] Ross, A. J., Edwards, G. F., and Waterfall, A. F., "The Dynamic Stability Derivatives of a Slender Wing at Zero and Moderate Lift. A Comparison of Theory with Free-Flight Model Tests, $M=0.8$ to 2.0," Aeronautics Research Council, Great Britain, C.P. No. 1310, 1973.

[25] Malvestuto, F. S. and Hoover, D. M., "Lift and Pitching Derivatives of Thin Sweptback Tapered Wings with Streamwise Tips and Subsonic Leading Edges at Supersonic Speeds," NACA TN 2294, 1951.

[26] Malvestuto, F. S. and Hoover, D. M., "Supersonic Lift and Pitching Moment of Thin Sweptback Tapered Wings Produced by Constant Vertical Acceleration, Subsonic Leading Edges, and Supersonic Trailing Edges," NACA TN 2315, 1951.

[27] Garner, H. C., "Multhopp's Subsonic Lifting-Surface Theory of Wings in Slow Pitching Oscillations," Aeronautics Research Council, Great Britain, R&M No. 2885, 1952.

[28] Woodgate, L., "Measurements of the Oscillatory Pitching Moment Derivatives on a Delta Wing with Rounded Leading Edges in Incompressible Flow," Aeronautics Research Council, Great Britain, R&M No. 3628, Pt. 1, 1968.

[29] Schneider, C. P., "Instationäre Flugkörper-Aerodynamik," Messerschmitt-Bölkow-Blohm, West Germany, MBB Bericht Nr. UA-306-75, 1975.

[30] Wendtz, W. H. Jr. and McMahon, M. C., "An Experimental Investigation of the Flow Fields About Delta and Double-Delta Wings at Low Speeds," NASA CR-521, 1967.

[31] Reding, J. P. and Ericsson, L. E., "Unsteady Aerodynamic Flow Field Analysis of the Space Shuttle Configuration Part II: Launch Vehicle Aeroelastic Analysis," NASA CR 144,333, April 1976.

[32] Reding, J. P. and Ericsson, L. E., "Effects of Flow Separation on Shuttle Longitudinal Dynamics and Aeroelasticity Stability," *Journal of Spacecraft and Rockets*, Vol. 14, Dec. 1977, pp. 711-718.

[33] Reding, J. P. and Ericsson, L. E., "Review of Delta Wing Shuttle Vehicle Dynamics," *Proceedings Space Shuttle Aerothermodynamics Conference*, Vol. III, NASA/AMES Research Center, Moffett Field, Calif., Dec. 15-16, 1971, NASA TM-X-2508, pp. 861-931.

[34] Allen, E. C., "An Investigation to Verify the Static Stability and Control Characteristics of the 0.004 Scale Model (74-0) of the Shuttle 5 Orbiter (0A108)," NASA CR 141,537, June 1975.

[35] Garner, H. C. and Bryer, D. W., "Experimental Study of Surface Flow and Part-Span Vortex Layers on a Cropped Arrowhead Wing," Aeronautics Research Council, Great Britain, R&M No. 3107, 1957.

[36] Boyden, R. P. and Freeman, D. C., "Subsonic and Transonic Dynamic Stability Derivatives of a Modified 089B Shuttle Orbiter," NASA TM X-72631, DMS-OR-2107, Dec. 1974.

[37] Ericsson, L. E., "Separated Flow Effects on the Static and Dynamic Stability of Blunt Nosed Cylinder-Flare Bodies," NASA CR 76, 919, Dec. 1965.

[38] Ericsson, L. E., "Unsteady Aerodynamics of Separating and Reattaching Flow on Bodies of Revolution," *Recent Research on Unsteady Boundary Layers*, Vol. 1, IUTAM Symposium, Laval University, Quebec, May 1971, pp. 481-512.

[39] Ericsson, L. E. and Reding, J. P., "Unsteady Aerodynamic Flow Field Analysis of the Space Shuttle Configuration, Part I, Orbiter Aerodynamics," NASA CR 144,332, April 1976.

[40] Sparks, V. H. and Moser, M. M. Jr., "Wind Tunnel Tests of an 0.015 Scale Configuration 140 A/B Space Shuttle Orbiter Model (67-0) in the NASA LRC 8-Foot TPT to Obtain Transonic Aerodynamic Force Data (OA-106)," NASA CR 134, June 1975.

[41] Ericsson, L. E. and Reding, J. P., "Scaling Problems in Dynamic Tests of Aircraft Like Configurations," *AGARD Symposium on Unsteady Aerodynamics*, Ottawa, Canada, Sept. 26-28, 1977.

[42] Ericsson, L. E. and Reding, J. P., "Reynolds Number Criticality in Dynamics Tests," AIAA Paper 78-166, AIAA 16th Aerospace Sci. Meet., Huntsville, Ala., Jan. 1978.